ADVANCED MATERIALS
www.advmat.de

Integration of Nanoassembly Functions for an Effective Delivery Cascade for Cancer Drugs

Qihang Sun, Xuanrong Sun, Xinpeng Ma, Zhuxian Zhou, Erlei Jin, Bo Zhang, Youqing Shen, Edward A. Van Kirk, William J. Murdoch, Joseph R. Lott, Timothy P. Lodge, Maciej Radosz, and Yuliang Zhao**

Cancer nanomedicine is regarded as one of the few strategies that may revolutionize cancer treatments.[1] Several nanomedicines such as DOXIL are in clinical use, and many more are under clinical trials.[2] A cancer nanomedicine delivering active drugs to the cytoplasm of cancer cells in a solid tumor must go through a cascade of five steps, i.e., circulation in the blood compartments (C), accumulation in the tumor via the enhanced permeability and retention (EPR) effect (A),[3] subsequent penetration deep into the tumor tissue (P), internalization by tumor cells (I), and finally intracellular drug release (R)—abbreviated as the CAPIR cascade (**Figure 1**a). Thus, a nanosystem would produce high therapeutic efficacy and good prognosis only if it efficiently accomplishes the full CAPIR cascade.[4] This may account for the difficulty of current nanomedicines[5]—they fail to or only marginally improve the overall survival of patients even though they deliver more anticancer agents to tumor tissues than free drugs.[6] For example, DOXIL effectively accumulates in the tumor tissues but cannot penetrate in the tumor, resulting in low therapeutic efficacy.[7] In our approach of integrating the functions of various materials, we made a cluster-bomb-like nanocarrier that synergizes the various functions of its components, thereby enabling it to complete the CAPIR cascade and achieve high therapeutic efficacy.

Q. Sun,[+] X. Sun,[+] Y. Shen, Y. Zhao
Center for Bionanoengineering and Key Laboratory of Biomass Chemical Engineering of Ministry of Education
Department of Chemical and Biological Engineering
Zhejiang University
Hangzhou, China 310027
E-mail: shenyq@zju.edu.cn; zhaoyl@nanoctr.cn

Q. Sun, X. Ma, Z. Zhou, E. Jin, B. Zhang, M. Radosz
Department of Chemical Engineering
University of Wyoming
Laramie, WY, USA 82071

E. A. Van Kirk, W. J. Murdoch
Department of Animal Science
University of Wyoming
Laramie, WY, USA 82071

J. R. Lott, T. P. Lodge
Department of Chemistry
University of Minnesota
Minneapolis, MN, USA 55455

Y. Zhao
National Center for Nanoscience and Technology
No.11, Beiyitiao Zhongguancun, Beijing, China 100190
[+]These authors contributed equally to this work.

DOI: 10.1002/adma.201401554

The utmost challenge in the design of a CAPIR-capable nanocarrier is the integration of the necessary functions into a single system since the required functions may be opposite in different CAPIR steps. For example, PEGylation[8] (PEG = poly(ethylene glycol)) and other designs[9] enable nanocarriers to be stealthy and thus long circulating, but these strategies substantially hinder their ability for cellular internalization.[10] Introducing targeting ligands[11] or cationic charges to nanocarriers promotes their cellular uptake,[12] but these techniques may greatly shorten the carrier's blood circulation and impede tumor penetration.[13] Nanoparticles of 100 nm have longer blood circulation times and better tumor accumulation than smaller particles,[14] but they are too large to diffuse into tumor tissues composed of tightly packed cells in a dense extracellular matrix.[7,15] Small nanocarriers can penetrate tumors,[4,16] but very small particles have short-lived blood circulation.[17] Many stimuli-responsive[18] or recent multistage nanosystems[19] have tried to accommodate the required opposing functions with various strategies: PEGylation and dePEGylation,[20] a large-to-small size transition,[21] or a negative-to-positive charge transition,[22] all of which are triggered by tumor microenvironment. None of these previously reported nanosystems, however, could simultaneously integrate all of the necessary opposing functions into one system.

We accommodated the opposing functions using a dendrimer–lipid nanoassembly that undergoes the three needed transitions for the CAPIR cascade similar to the way a cluster bomb undergoes two stage-actions; the nanoassembly accomplishes the missions of blood circulation and tumor accumulation (the CA steps of CAPIR), while its small nanocarrier components act as "bomblets" accomplishing the missions of tumor penetration and cell internalization as well as drug release (the PIR steps of CAPIR) (Figure 1b). Lipids are most clinically used for formulating drug delivery nanocarriers[23] and recently also used as coatings for nanostructures.[24] Hence a fusogenic phospholipid DOPE (1,2-dioleoyl-*sn*-glycero-3-phosphoethanolamine) was chosen to coat the dendrimers, but it was expected to peel off by fusion once inside tumor tissue. A PEGylated lipid DSPE-PEG (DSPE = 1,2-distearoyl-*sn*-glycero-3-phosphoethanolamine) and cholesterol (Figure 1c) were added to make the nanoassembly stealthy and stable in the blood. Dendrimers were chosen as the "bomblets" because of their monodispersity, uniform nanoscale size, and ability to carry anticancer drugs.[25] A sixth-generation nontoxic degradable polyaminoester dendrimer with a diameter of 5 nm was synthesized (Figure 1c)[26] with pH-dependent 2-(*N,N*-diethylamino)ethyl termini. The

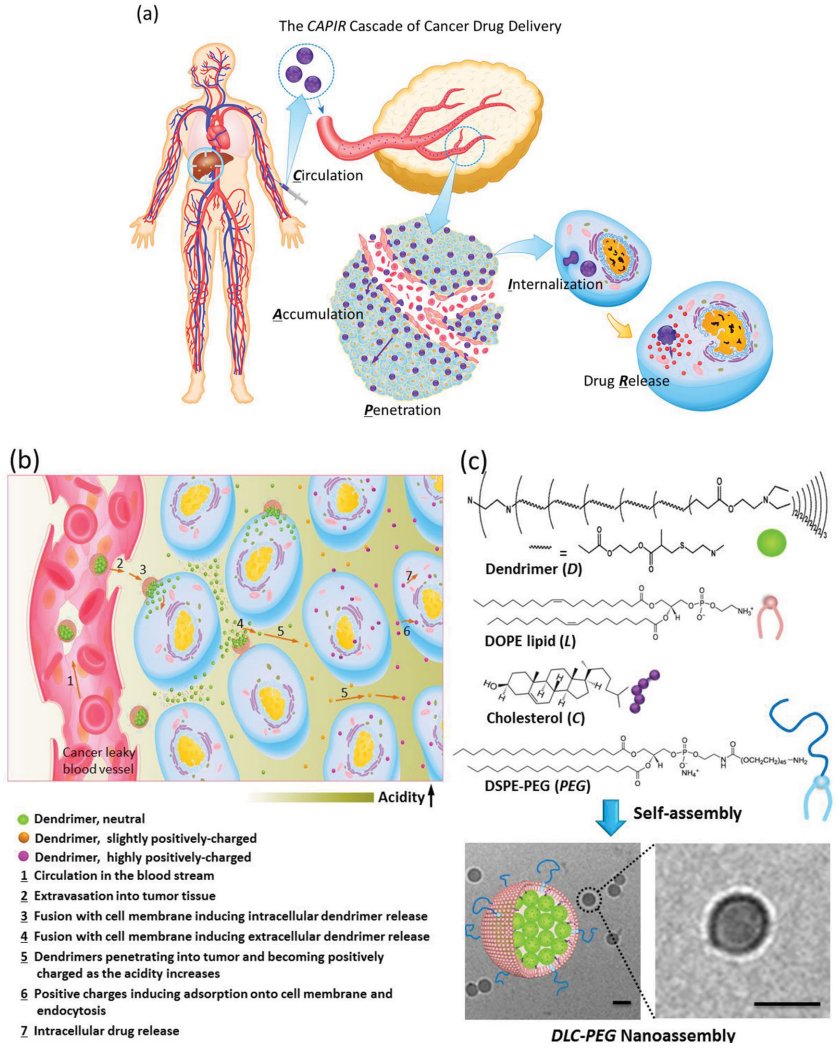

Figure 1. The CAPIR cascade of cancer drug delivery and the liposomal dendrimer nanoassembly. a) Schematic of the *CAPIR* cascade, a cascade of five steps in cancer drug delivery, i.e., circulation in the blood compartments, tumor accumulation and penetration, and subsequent cellular internalization and intracellular drug release. b) Schematic of the cluster-bomb-like nanoassembly and how it accomplishes the CAPIR cascade. The nanoassembly is a surface-PEGylated lipidic nanoassembly of 5-nm pH-responsive dendrimers. It circulates in the blood compartments and accumulates in the tumor via the EPR effect. Once in the tumor, fusion of the lipid layer with the cell membrane releases the dendrimers intracellularly or extracellularly. The small nearly neutral dendrimers in the extracellular fluid penetrates further into tumor tissues, where the extracellular pH is acidic (pH = ~6–7). The dendrimers are then protonated and became positively charged, efficiently triggering fast cellular uptake and bypassing the membrane-associated drug-resistance mechanisms. c) The nanoassembly structure: the dendrimers were self-assembled with DOPE and DSPE-PEG lipids as well as cholesterol to form the nanoassembly with a dendrimer core and lipidic shell, which was confirmed by cryo-TEM imaging. Scale bar = 50 nm.

zeta-potential was 2.2 mV at pH 7.4 and 7.0 mV at pH 6.5 in 0.2 M phosphate buffered saline (PBS) solution (Figure S1, Supporting Information (SI)). Thus, the dendrimer can be quickly internalized at acidic pH (SI: Figure S2), thereby shipping the drugs into the cytosol and circumventing the cell's multidrug resistance (SI: Figure S3, S4). Furthermore, the dendrimer's core is hydrophobic at neutral pH, but it becomes water-soluble at a pH of ~6 because it contains many tertiary amines in its backbone. Thus, hydrophobic drugs could be encapsulated inside the dendrimer at neutral pH and released once at lower pH.[27]

The self-assembly of the dendrimer with DOPE lipid, cholesterol, and DSPE-PEG (abbreviated as D, L, C, and PEG, respectively, in the nanoassembly label: DLC-PEG) was fine-tuned in terms of the size, zeta-potential, and stability (SI: Figure S5). The optimum PEGylated DLC-PEG nanoassembly was obtained at a D:L:C:PEG molar ratio of 1:60:60:1.5 with a size of 30 ± 2 nm (polydispersity index, PDI = 0.163) and zeta-potential of –9.1 ± 0.5 mV. The structure of the DLC-PEG nanoassembly was probed by regular and cryogenic transmission electron microscopy (TEM and cryo-TEM, respectively). As illustrated in Figure 1c (and in the SI: Figure S6), both regular TEM (with negative staining using hydrophilic uranyl acetate) and cryo-TEM images showed a dim ring surrounding a bright core, indicating a hydrophobic core surrounded by a hydrophilic layer. Assuming no deformation occurred when the dendrimers packed together, it was therefore estimated that the DLC-PEG nanoassembly (30 nm in diameter) roughly contained 27 dendrimers (5 nm in diameter) aggregated together and coated with a lipid monolayer.

The nanoassembly structure was further probed using a fluorescence quenching approach. A fluorescent FITC-tethered dendrimer (FITC = fluorescein isothiocyanate; ^{FITC}D = tethered dendrimer; SI: Figure S7a,b) was used to fabricate the labeled nanoassembly ^{FITC}DLC-PEG. Gold nanoparticles (AuNPs, 4 nm, see SI: Figure S7c) are known to quench the FITC fluorescence and are too big to diffuse through a lipid layer. Thus, the fluorescence of free ^{FITC}dendrimer in solution was gradually quenched upon addition of AuNPs (SI: Figure S7d,e). However, adding AuNPs to the ^{FITC}*DLC-PEG* nanoassembly solution only slightly reduced the fluorescence intensity (SI: Figure S7f). This suggests that most of the FITC were inaccessible to the 4-nm AuNPs, further confirming that most of the ^{FITC}D (82%) were encapsulated by a lipid layer within the nanoassembly structure.

An anticancer drug doxorubicin (DOX) was loaded into the DLC-PEG nanoassembly. The resulting DLC-PEG/DOX had a slightly larger diameter, 45 ± 5 nm, and a DOX-content of 9 ± 2 wt%. The DLC-PEG/DOX could be lyophilized with trehalose—a known lyoprotectant reagent (DLC-PEG:trehalose w/w ratio = 1/12)—and easily redispersed in aqueous solution with almost no effect on its size. The DOX-loaded DLC-PEG released DOX more slowly than the unbound dendrimers

Adv. Mater. **2014**,
DOI: 10.1002/adma.201401554

and the dendrimer-free assembly of *LC-PEG*, indicating that DOX was primarily encapsulated in the dendrimers (SI: Figure S8). Although the release profile was still not ideal, changing the dendrimer to one that can hold DOX more tightly has the potential to greatly suppress premature release.

The cellular uptake of DLC-PEG into cells of the SKOV-3 cell line (human ovarian cancer cells) was observed using confocal microscopy. The ^{FITC}D (green signal) and some DOPE labeled with rhodamine B (^{RHoB}L, red signal) were employed to form the dual-labeled nanoassembly $^{FITC}D^{RHoB}$*LC-PEG* (yellow spots). After $^{FITC}D^{RHoB}$*LC-PEG* was incubated with cells for 4 h, the free dendrimer, free lipid, and the nanoassembly were found attached to the cell membrane (**Figure 2**a). After 12 h incubation, the lipids were still on the cell membrane, but the dendrimers were found inside the cells, suggesting that the nanoassembly dissociated and released the dendrimers. Furthermore, the DOX in the DLC-PEG nanoassembly was in the cytoplasm after 12 h incubation (SI: Figure S9). Notably, dendrimer/DOX (red signal), which was delivered by the nanoassembly, was not localized in the lysosomes (green signal) (Figure 2b). In contrast, the cultured free dendrimers were found in lysosomes (SI: Figure S10). The effects of temperature and endocytosis pathway inhibitors (chlorpromazine, filipin III, and wortmannin) on the cellular uptake of the nanoassembly were probed by flow cytometry (Figure 2c). Cellular uptake was suppressed to half at 4 °C, suggesting that the internalization was mainly energy-dependent. The presence of chlorpromazine, filipin III, or wortmannin had almost no effect on the cellular uptake of the nanoassembly. A similar result was obtained when adding cytochalasin D, a commonly used inhibitor of actin-polymerization for phagocytosis (SI: Figure S11). The results indicate that cellular uptake of the nanoassembly was not through the common endocytosis, macropinocytosis, or phagocytosis pathways.

We used DOPE for its fusion capability to induce the disassembly of DLC-PEG after interacting with tumor cells and probed it by a fluorescence-resonance energy-transfer (FRET) approach.[28] DOPE lipids were separately labeled with a pair of FRET dyes, RHoB and NBD (^{RHoB}DOPE and ^{NBD}DOPE), and mixed with DOPE at a DOPE:^{RHoB}DOPE:^{NBD}DOPE molar ratio of 94:1:5 to form the nanoassembly with dual-labeled lipid, $D^{RHoB/NBD}$LC-PEG (Figure 2d). If the lipid layer fuses with the cell membrane, the ^{RHoB}DOPE/^{NBD}DOPE lipids will migrate to the cell membrane and separate, inhibiting their FRET. A FRET efficiency index, *R*, can be calculated from the intensity ratio of the ^{RHoB}DOPE fluorescence at 585 nm to the ^{NBD}DOPE

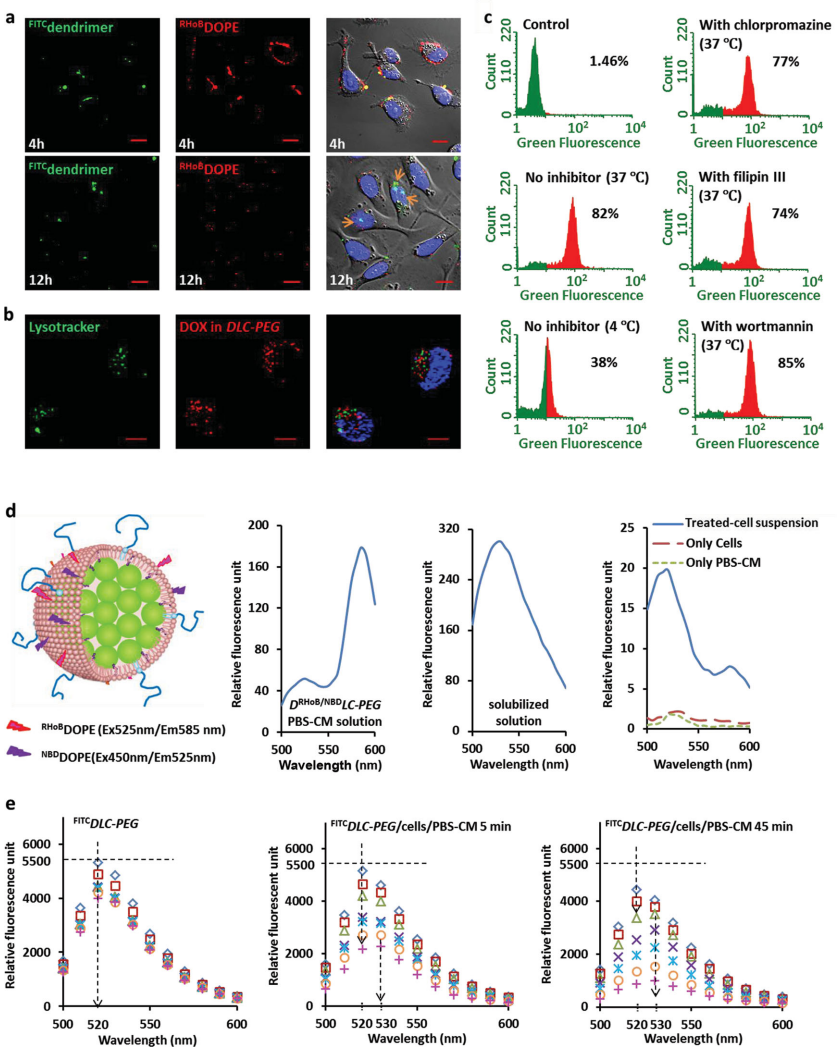

Figure 2. a–c) Cellular internalization and intracellular localization and d,e) fusion with cell membrane causing extracellular dendrimer release of the DLC-PEG nanoassembly. a) Confocal images of cellular uptake of DLC-PEG into SKOV-3 ovarian cancer cells. The cells were treated with dual-labeled $^{FITC}D^{RHoB}$LC-PEG for 4 or 12 h. ^{FITC}D is shown in green; ^{RHoB}L mixed in the DOPE lipid layer is shown in red, and cell nuclei are stained with Draq 5 in blue. All scale bars are 10 μm. b) Subcellular localization of DLC-PEG/DOX. The SKOV-3 cells were treated with DLC-PEG/DOX at a DOX-equivalent dose of 0.8 μg/mL for 6 h. Lysotracker-dyed lysosomes are shown in green, and DOX loaded in DLC-PEG is shown in red. All scale bars are 10 μm. c) FITC-positive SKOV-3 cells measured by flow cytometry after treatment with ^{FITC}DLC-PEG for 6 h at different temperatures or at 37 °C in the presence of inhibitors. The FITC-equivalent dose was 60 μg/mL. d) Fusion assay using a FRET approach. The DLC-PEG lipid layer was dual-labeled with ^{NBD}DOPE (excitation and emission wavelengths: Ex = 450 nm, Em = 525 nm) and ^{RHoB}DOPE (Ex = 525 nm, Em = 585 nm) at a DOPE:^{RHoB}DOPE:^{NBD}DOPE molar ratio of 94:1:5. Fluorescence emission spectra of different solutions were recorded by a 450 nm laser for excitation. The PBS-CM solution was PBS containing 0.36 mM calcium and 0.42 mM magnesium. e) Dendrimer extracellular release into the extracellular medium from DLC-PEG. The release was induced by cell membrane fusion and measured by an FITC-fluorescence quenching method. SKOV-3 cells (2.5×10^5) were incubated with ^{FITC}DLC-PEG PBS-CM solution at 37 °C for 5 or 45 min (the spectra at other time intervals are in the SI: Figure S12), and then the FITC fluorescence of the supernatant cell culture medium was measured before and after adding different amounts of AuNPs (1 mg/mL solution added in the following amounts; 0 (◇), 10 (□), 20 (△), 40 (×), 60 (✳), 80 (○), and 100 (+) μL).

fluorescence at 525 nm when excited at 450 nm.[29] Upon excitation at 450 nm, the intact $D^{RHoB/NBD}$LC-PEG nanoassembly had a strong FRET-fluorescence peak at 585 nm and a weak peak at 525 nm with an *R* value of 3.4 (*R* = 178.6/51.9). In the solubilized control solution, the addition of 0.24 vol% Triton X-100 led to the nanoassembly dissolving and dissembling, completely eliminating FRET. Interestingly, the cells treated with the $D^{RHoB/NBD}$LC-PEG nanoassembly had very strong florescence at 525 nm but a very weak FRET peak with an *R* value of 0.39 (*R* = 7.79/19.81; Figure 2d, right), indicating that many of the nanoassembly lipids were in the cell membrane but that they had separated. This finding is in agreement with the confocal microscopy observations and with the flow cytometry results (Figure 2a,c), in which the nanoassembly fused with the cell membrane and released the dendrimers directly into the cytoplasm.

The (lipid layer)–(cell membrane) fusion was also designed to strip off the lipid layer from the DLC-PEG nanoassembly to extracellularly release the dendrimers for penetration into the tumor. Since tumor tissues are tightly packed with cells in a dense extracellular matrix, this fusion would be more feasible than that in blood. To test the extracellular dendrimer release, we incubated ^{FITC}*DLC-PEG* with high-density SKOV-3 cells (2.6×10^4 cells/cm^2) at 37 °C and collected the extracellular culture medium. The ^{FITC}D fluorescence in the medium was measured, and the nanoassembly integrity was probed again using the AuNP quenching method (Figure 2e and SI: Figure S12). After the nanoassembly was incubated with the cells for 5 min, some ^{FITC}D fluorescence became quenchable by the AuNPs, and the peak FITC emission shifted from 520 to 530 nm, which is typical for FITC in a hydrophilic environment. This phenomenon became much more pronounced after longer incubation. After 45 min of incubation, the ^{FITC}D fluorescence was completely quenched after adding 100 µL of the AuNP solution, which is very similar to free ^{FITC}D, indicating that the dendrimers in the extracellular solution were in an aqueous environment. Therefore, it can be concluded that the lipid layer of the nanoassembly could fuse with the cell membrane, releasing the dendrimers either into the cell cytosol or the extracellular medium as we had intended (Figure 1b).

The cytotoxicity of the DOX loaded in DLC-PEG (DLC-PEG/DOX) to five cancer cell lines was slightly lower than that of free DOX (SI: Figure S13), suggesting that DOX was not taken into lysosomes but released into the cytosol to exert its efficacy. The blank, DLC-PEG without any DOX, had no cytotoxicity. Importantly, the cytosolic dendrimer/DOX remained in the cells and did not undergo exocytosis, whereas intracellular free DOX was quickly excluded from the cells within 10 h (SI: Figure S14), indicating that the dendrimer/DOX indeed could overcome the membrane-associated drug resistance.

Several tumor models were used to evaluate the nanoassembly's ability to accomplish the CAPIR process. The in-vivo stealthy property of DLC-PEG was first compared with a standard long-circulating nanocarrier of similar size,

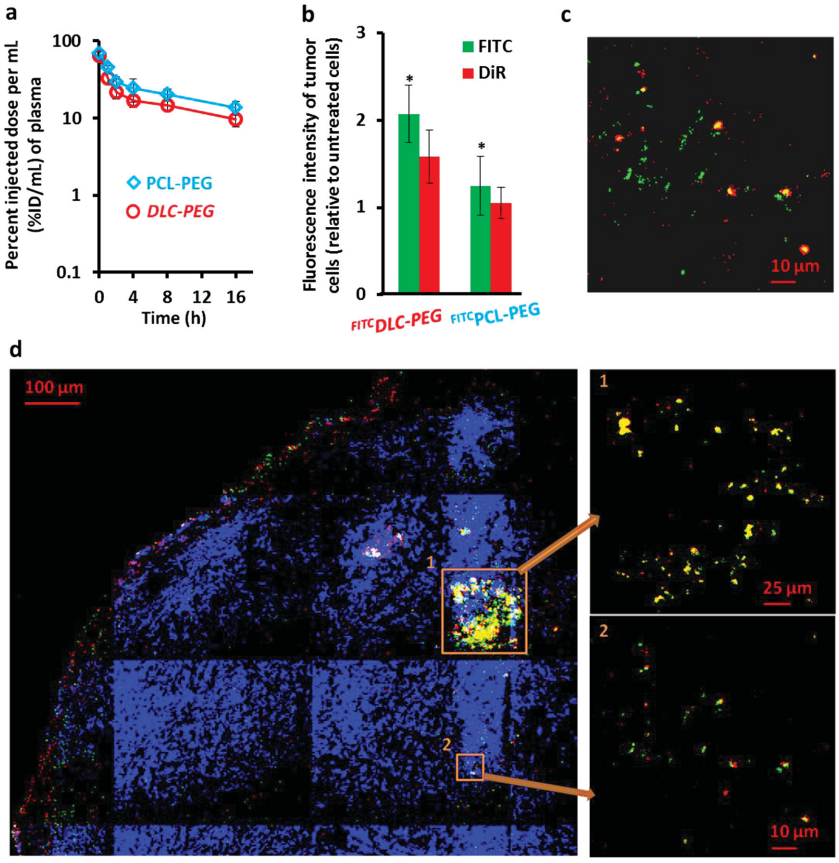

Figure 3. In-vivo blood clearance (a), tumor accumulation (b), dissociation (c), and tumor distribution (d) of the DLC-PEG nanoassembly. a) Blood clearance of DiR-loaded DLC-PEG nanoassembly and PCL-PEG micelles in female athymic mice after a single dose of 0.15 mg of DiR per kilogram of body weight. Error bars represent standard deviation of means ($n = 3$). b) The accumulation of DiR-loaded ^{FITC}DLC-PEG nanoassembly and $^{FITC}PCL_{2.5k}$-PEG_{5k} micelles in tumor cells in terms of the averaged fluorescence intensity of tumor cells. The fluorescence-positive cells were analyzed by flow cytometry for FITC (ex = 488 nm, em = 530 nm) or DiR (ex = 710 nm, ex = 760 nm). The florescence intensity of tumor cells relative to untreated tumor cells was obtained by integrating the area under the curve of the plot (cell count against florescence intensity) divided by that of the control cells (SI: Figure S17). *, P = 0.038. c,d) The dissociation and intratumoral distribution of DiR-loaded ^{FITC}D- and ^{RHoB}DOPE-labeled nanoassembly ($^{FITC}D^{RHoB}$*LC-PEG*/DiR) in SKOV-3 tumor tissue observed by confocal microscopy. The tumor tissue slides (10 µm thick) were sectioned from SKOV-3 tumor-bearing mice intravenously treated with the nanoassembly for 16 h after a single dose of 0.15 mg DiR per kilogram of body weight. In (c), the ^{FITC}D is shown in green and the ^{RHoB}DOPE-labeled lipid layer in red. In (d), the confocal image of a quarter of the whole slide was obtained by tile scan. The ^{FITC}D is shown in green, the DiR shown in red, and the DAPI for the cell nuclei shown in blue. The selected areas (1) and (2) were magnified and re-confocalized to diminish the blurry yellow dots with increased observatory contrast. The tile scan images of other tumor-tissue slides sectioned from mice treated with the controls (^{FITC}PCL-PEG/DiR) are available in the SI (Figure S18).

Adv. Mater. **2014**,
DOI: 10.1002/adma.201401554

polycaprolactone-*block*-PEG (PCL-PEG; sometimes subscripts are included to indicate the size of each block) micelles. Both the dendrimers in the nanoassembly and the PCL-PEG (the PCL end) were conjugated with FITC for non-leaching labeling. A hydrophobic fluorescence probe, DiR, was loaded as a model drug into ^{FITC}DLC-PEG and ^{FITC}PCL-PEG for tracing because the fluorescence wavelengths of DOX and FITC partially overlap. DiR- and DOX-loaded DLC-PEG had similar sizes, blood circulation times, biodistributions, and extraction efficiencies (SI: Figure S15).

DLC-PEG/DiR was found to circulate in the blood in a similar manner as the well-known long-circulating PCL-PEG/DiR micelles, suggesting that the nanoassembly was stable in blood and indeed had good stealthiness (**Figure 3**a). Their biodistribution profiles in the liver, spleen, and kidneys were not significantly different at 16 h post-injection, but significantly different in the tumor, lung, and blood (SI: Figure S16). DLC-PEG/DiR accumulated more in the tumor cells than PCL-PEG/DiR in terms of the overall fluorescence intensity of either FITC or the DiR in the tumor cells. The amount of ^{FITC}D accumulated in tumor cells was 1.7 (statistical *P*-value of $P = 0.038$) times that of FITC-labeled PCL-PEG; similarly, the amount of DiR-loaded DLC-PEG accumulated in the tumor was 1.5 times that of the DiR-loaded PCL-PEG (Figure 3b and SI: Figure S17).

The dual-labeled ^{FITC}D^{RHoB}LC-PEG nanoassembly was loaded with DiR (^{FITC}D^{RHoB}LC-PEG/DiR) and used to observe the intratumoral distribution, nanoassembly dissociation, and drug release (Figure 3c). The ^{FITC}D (green signal) was separate from the ^{RHoB}DOPE (red signal), suggesting dissociation of the dendrimers and lipid layer in the tumor. The green signal of the ^{FITC}D and red signal of DiR in Figure 3d mostly overlapped as yellow spots after the nanoassembly extravasated from the blood vessel into the tumor (Figure 3, magnified area 1), and they mostly overlapped during deep penetration through the tumor tissue (Figure 3, magnified area 2), indicating that the dendrimers retained DiR well. Furthermore, the dendrimers distributed throughout the tumor (Figure 3d, large view). We further examined the tumor accumulation and penetration of DOX delivered by DLC-PEG in BCAP-37 and MCF-7 tumor-bearing mice and compared them with similar-sized PCL_{2k}-PEG_{2k}/DOX nanoparticles (40 nm in diameter). The DLC-PEG delivered 1.7 ($P < 0.05$) times as much DOX as PCL_{2k}-PEG_{2k} (**Figure 4**a), similar to the DiR result (1.9-fold, $P < 0.05$; SI: Figure S19). The confocal image of a tumor slice clearly showed that DOX was much more homogeneously distributed in the tumor, whereas the DOX delivered by PCL_{2k}-PEG_{2k} was mostly retained in the invasive edge (Figure 4b,c). The calculated DOX intensity (I_{DOX}) inside the tumor treated with DLC-PEG/DOX was about 10 times more than that treated with PCL_{2k}-PEG_{2k}/DOX (Figure 4b). Similar results were found in the MCF-7 tumor model (SI: Figure S20). These results further prove that the nanoassembly DLC-PEG could release the dendrimers once in the tumor, and the small dendrimers penetrated more deeply into the whole tumor tissue.

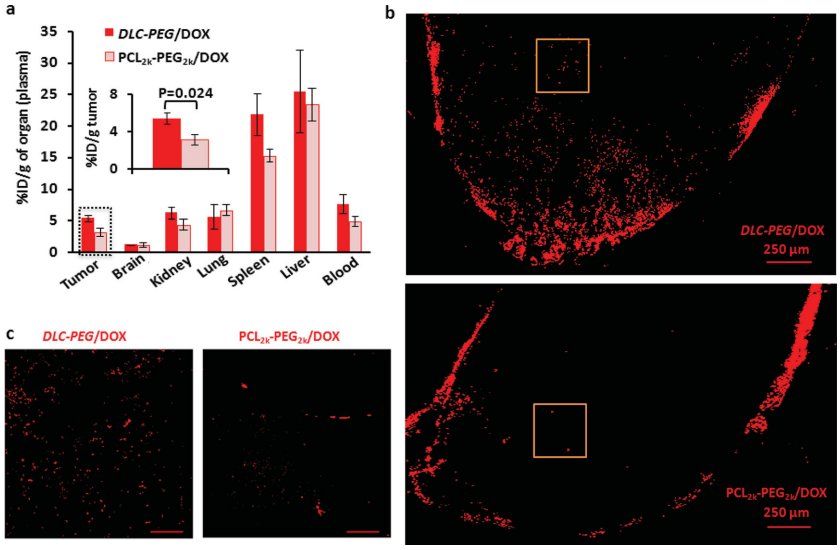

Figure 4. DOX biodistribution and intratumoral distribution of DLC-PEG/DOX and PCL_{2k}-PEG_{2k}/DOX. a) Biodistribution of DLC-PEG/DOX (45 nm) and PCL_{2k}-PEG_{2k}/DOX (40 nm) in BCAP-37 tumor-bearing mice 16 h after a single injection of 1.0 mg DOX per kilogram of body weight. The inset is a magnified view of the DOX accumulated in the tumor. Error bars represent the standard deviation ($n = 3$). b) Confocal images obtained by a tile scan of the slides (10 μm thick) sectioned from the treated BCAP-37 tumors. DOX is shown in red. Magnified views of the selected areas in (b) are shown in (c). Scale bar is 50 μm. The DOX fluorescence intensity (I_{DOX}) inside the tumor excluding the edges (the area inside the dotted lines) was obtained with arbitrary units by integration of the DOX fluorescence using MATLAB.

The in-vivo therapeutic efficacy of DLC-PEG/DOX was compared with the micellar PCL-PEG/DOX using subcutaneous tumor-bearing mice of a well-established cancer cell line pair, drug-sensitive/resistant MCF-7 and MCF-7/ADR breast cancer cells (**Figure 5**a; SI: Figure S21 and S22). The DLC-PEG/DOX lyophilized with trehalose was redissolved in pure water to appropriate doses. Thus, all other treatments were also administered in the same trehalose solution (60 mg/mL), and the trehalose solution was used as a control. Clearly, DLC-PEG/DOX and free DOX inhibited the growth of drug-sensitive MCF-7 tumors completely, much more efficiently than PCL_{2k}-PEG_{2k}/DOX ($P < 0.005$). On day 19, DLC-PEG/DOX had an 85% tumor inhibition rate in terms of tumor weight, much higher than PCL_{2k}-PEG_{2k}/DOX (40%). Hematoxylin–eosin (H&E) staining (Figure 5b) showed that tumors treated with trehalose or the blank nanoassembly consisted of typical, tightly packed tumor cells, whereas those treated with DOX or DLC-PEG/DOX exhibited extensive vacuolization. TUNEL staining (TdT-mediated dUTP nick end labeling) confirmed that most MCF-7 tumor cells treated with DLC-PEG/DOX or DOX were TUNEL-positive (brown staining) and scored as apoptotic, but fewer apoptotic cells were found in tumors treated with PCL_{2k}-PEG_{2k}/DOX.

When used for treatment of drug-resistant MCF-7/ADR tumor-bearing mice, free DOX or PCL_{2k}-PEG_{2k}/DOX could not inhibit the tumor growth anymore ($P > 0.05$ compared

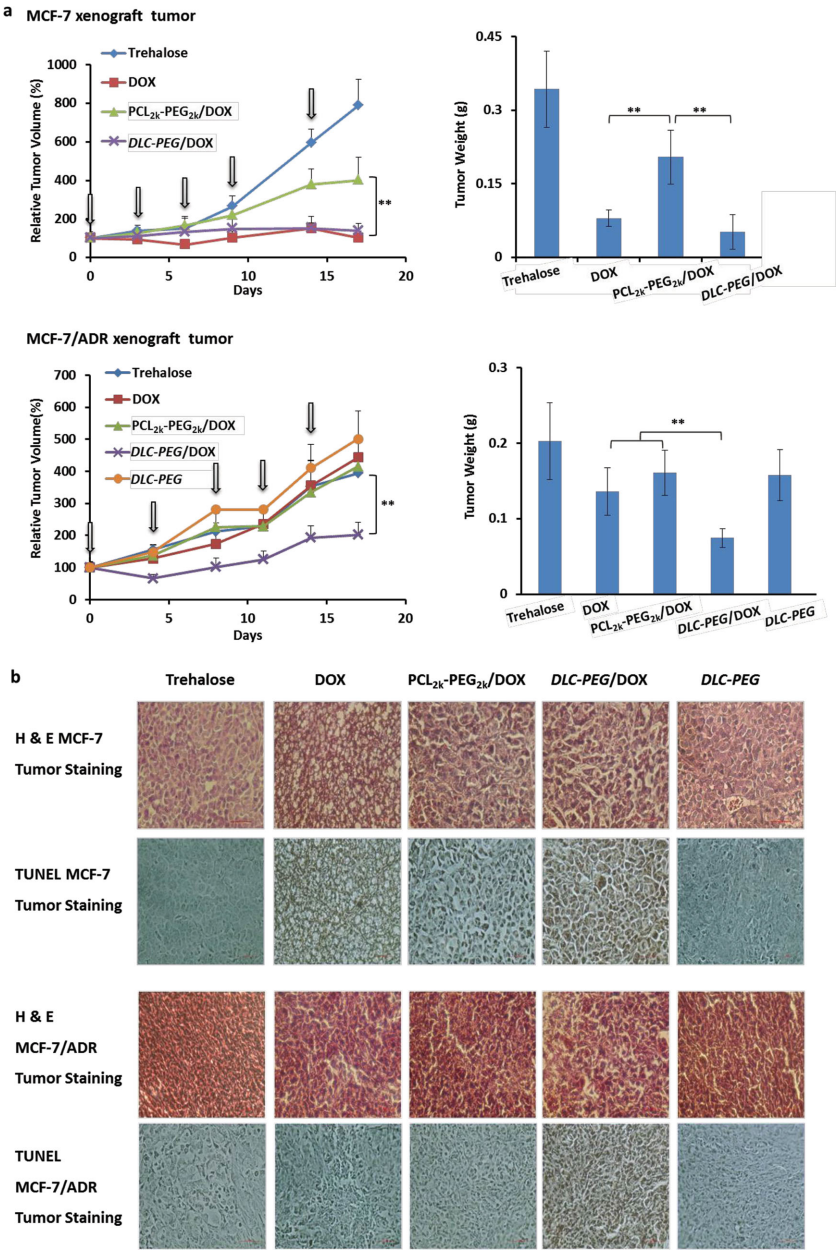

Figure 5. In-vivo antitumor activity of DLC-PEG/DOX (a) and H&E and TUNEL tumor staining of the MCF-7 and MCF-7/ADR tumor-bearing mice (b). a) MCF-7 and MCF-7/ADR xenografted nude mice were administered with the treatments intravenously at a DOX-equivalent dose of 4 mg/kg every two or three days as indicated by the arrows; each tumor was measured at the time of the injection and its relative tumor volume was calculated ($n = 6$, data expressed as average ± standard error). On day 19, the mice were terminated and the tumors were dissected and weighed; ** $P < 0.005$. b) Tissue paraffin sections were 10 μm thick. The tumor sections were stained with hematoxylin–eosin and examined by light microscopy. The TUNEL assay was used to determine the apoptotic cells in situ in the dissected tumor tissue slides. Apoptotic cells were identified by positive TUNEL staining (brown) under light microscopy.

with the trehalose group), whereas DLC-PEG/DOX almost completely stopped the tumor growth, and the difference was more significant ($P < 0.005$) after day 17 (Figure 5a). On day 19, DLC-PEG/DOX had a tumor inhibition rate of 63%, but it was only 32% for DOX and 21% for PCL_{2k}-PEG_{2k}/DOX, which were similar to the control. H&E and TUNEL staining (Figure 5b) showed that the MCF-7/ADR tumors treated with DLC-PEG/DOX consisted mostly of apoptotic cells, but such cells were rare in those treated with PCL_{2k}-PEG_{2k}/DOX or DOX.

Coupled with the tumor penetration results as discussed above, the difference in therapeutic efficacy suggests that DOX could not get into the drug-resistant cells and had low efficacy. PCL-PEG micelles could circumvent the membrane-associated drug resistance via endocytosis and take DOX into drug-resistant cells,[30] but it could not penetrate into the tumor tissue to reach cells away from the tumor blood vessels. In contrast, DLC-PEG/DOX released the drug-loaded dendrimers, which further penetrated deep in tumor tissues. Importantly, the dendrimers became positively charged in the acidic tumor extracellular fluids[31] and were efficiently internalized via endocytosis (SI: Figure S3, S4), circumventing the drug resistance and leading to significantly enhanced therapeutic efficacy, as sketched in Figure 1b. During the treatments, DOX caused a significant loss of mouse body weight and histological changes in the cardiomyocytes; in contrast, DLC-PEG/DOX treatment did not cause this weight loss, and the treated mice exhibited no differences in cardiomyocyte structures compared to trehalose- and blank-nanoassembly-treated mice (SI: Figure S23).

Supporting Information

Supporting Information is available from the Wiley Online Library or from the author.

Acknowledgements

This study was funded by the National Natural Science Foundation Key Program (51390481 and 21090352), the National Basic Research Program (2014CB931900), the National Fund for Distinguished Young Scholars (50888001), and the Doctoral Fund of Ministry of Education (20110101130007) of China, and the US Department of Defense (BC090502). Cryo-TEM characterizations were carried out in the Characterization Facility, University of Minnesota, which receives partial support from the NSF through the MRSEC program.

Received: April 6, 2014
Revised: September 3, 2014
Published online:

[1] a) T. M. Allen, P. R. Cullis, *Science* **2004**, *303*, 1818; b) R. K. Jain, T. Stylianopoulos, *Nat. Rev. Clin. Oncol.* **2010**, *7*, 653; c) J. W. Yoo, D. J. Irvine, D. E. Discher, S. Mitragotri, *Nat. Rev. Drug Discov.* **2011**, *10*, 521; d) J. Wu, Z. Li, *Chin. Sci. Bull.* **2013**, *58*, 4515.
[2] a) Z. Cheng, A. Al Zaki, J. Z. Hui, V. R. Muzykantov, A. Tsourkas, *Science* **2012**, *338*, 903; b) R. Tong, J. Chen, *Polym. Rev.* **2007**, *47*, 345.
[3] T. P. Padera, A. Kadambi, E. di Tomaso, C. M. Carreira, E. B. Brown, Y. Boucher, N. C. Choi, D. Mathisen, J. Wain, E. J. Mark, L. L. Munn, R. K. Jain, *Science* **2002**, *296*, 1883.
[4] V. P. Chauhan, R. K. Jain, *Nat. Mater.* **2013**, *12*, 958.
[5] Q. Sun, M. Radosz, Y. Shen, *J. Controlled Release* **2012**, *164*, 156.
[6] a) D. L. Stirland, J. W. Nichols, S. Miura, Y. H. Bae, *J. Controlled Release* **2013**, *172*, 1045; b) Y. Barenholz, *J. Controlled Release* **2012**, *160*, 117.
[7] F. Yuan, M. Leunig, S. K. Huang, D. A. Berk, D. Papahadjopoulos, R. K. Jain, *Cancer Res.* **1994**, *54*, 3352.
[8] S. Dufort, L. Sancey, J. L. Coll, *Adv. Drug Deliv. Rev.* **2012**, *64*, 179.
[9] a) P. L. Rodriguez, T. Harada, D. A. Christian, D. A. Pantano, R. K. Tsai, D. E. Discher, *Science* **2013**, *339*, 971; b) F. Alexis, E. Pridgen, L. K. Molnar, O. C. Farokhzad, *Mol. Pharm.* **2008**, *5*, 505.
[10] a) S. Mishra, P. Webster, M. E. Davis, *Eur. J. Cell Biol.* **2004**, *83*, 97; b) H. Hatakeyama, H. Akita, H. Harashima, *Adv. Drug Deliv. Rev.* **2011**, *63*, 152.
[11] a) N. Kamaly, Z. Y. Xiao, P. M. Valencia, A. F. Radovic-Moreno, O. C. Farokhzad, *Chem. Soc. Rev.* **2012**, *41*, 2971; b) J. O. Martinez, B. S. Brown, N. Quattrocchi, M. Evangelopoulos, M. Ferrari, E. Tasciotti, *Chin. Sci. Bull.* **2012**, *57*, 3961; c) X. Sun, J. Xu, J. Tang, M. Sui, Y. Shen, *Chin. J. Polym. Sci.* **2011**, *29*, 427.
[12] a) T. R. Pearce, K. Shroff, E. Kokkoli, *Adv. Mater.* **2012**, *24*, 3803; b) C. Xu, M. Sui, J. Tang, Y. Shen, *Chin. J. Polym. Sci.* **2011**, *29*, 274.
[13] a) A. I. Minchinton, I. F. Tannock, *Nat. Rev. Cancer* **2006**, *6*, 583; b) S. Mitragotri, J. Lahann, *Adv. Mater.* **2012**, *24*, 3717.
[14] S. D. Perrault, C. Walkey, T. Jennings, H. C. Fischer, W. C. W. Chan, *Nano Lett.* **2009**, *9*, 1909.
[15] H. Cabral, Y. Matsumoto, K. Mizuno, Q. Chen, M. Murakami, M. Kimura, Y. Terada, M. R. Kano, K. Miyazono, M. Uesaka, N. Nishiyama, K. Kataoka, *Nat. Nanotechnol.* **2011**, *6*, 815.
[16] N. Tang, G. Du, N. Wang, C. Liu, H. Hang, W. Liang, *J. Natl. Cancer Inst.* **2007**, *99*, 1004.
[17] a) H. S. Choi, W. Liu, F. Liu, K. Nasr, P. Misra, M. G. Bawendi, J. V. Frangioni, *Nat. Nanotechnol.* **2010**, *5*, 42; b) H. S. Choi, W. Liu, P. Misra, E. Tanaka, J. P. Zimmer, B. Itty Ipe, M. G. Bawendi, J. V. Frangioni, *Nat. Biotechnol.* **2007**, *25*, 1165.
[18] a) S. Mura, J. Nicolas, P. Couvreur, *Nat. Mater.* **2013**, *12*, 991; b) J. A. Hubbell, A. Chilkoti, *Science* **2012**, *337*, 303; c) Y. L. Colson, M. W. Grinstaff, *Adv. Mater.* **2012**, *24*, 3878; d) J. Wang, X. Sun, W. Mao, W. Sun, J. Tang, M. Sui, Y. Shen, Z. Gu, *Adv. Mater.* **2013**, *25*, 3670.
[19] a) B. Godin, E. Tasciotti, X. Liu, R. E. Serda, M. Ferrari, *Acc. Chem. Res.* **2011**, *44*, 979; b) C. Wang, Z. X. Li, D. Cao, Y. L. Zhao, J. W. Gaines, O. A. Bozdemir, M. W. Ambrogio, M. Frasconi, Y. Y. Botros, J. I. Zink, J. F. Stoddart, *Angew. Chem. Int. Ed.* **2012**, *51*, 5460.
[20] B. Romberg, W. E. Hennink, G. Storm, *Pharm. Res.* **2008**, *25*, 55.
[21] a) E. Tasciotti, X. W. Liu, R. Bhavane, K. Plant, A. D. Leonard, B. K. Price, M. M. C. Cheng, P. Decuzzi, J. M. Tour, F. Robertson, M. Ferrari, *Nat. Nanotechnol.* **2008**, *3*, 151; b) C. Wong, T. Stylianopoulos, J. A. Cui, J. Martin, V. P. Chauhan, W. Jiang, Z. Popovic, R. K. Jain, M. G. Bawendi, D. Fukumura, *Proc. Natl. Acad. Sci. USA* **2011**, *108*, 2426.
[22] a) J. Z. Du, T. M. Sun, W. J. Song, J. Wu, J. Wang, *Angew. Chem. Int. Ed.* **2010**, *49*, 3621; b) E. Jin, B. Zhang, X. Sun, Z. Zhou, X. Ma, Q. Sun, J. Tang, Y. Shen, E. Van Kirk, W. J. Murdoch, M. Radosz, *J. Am. Chem. Soc.* **2013**, *135*, 933.
[23] a) T. M. Allen, P. R. Cullis, *Adv. Drug Deliv. Rev.* **2013**, *65*, 36; b) S. Singh, A. Sharma, G. P. Robertson, *Cancer Res.* **2012**, *72*, 5663; c) T. R. Pearce, K. Shroff, E. Kokkoli, *Adv. Mater.* **2012**, *24*, 3803.
[24] a) C. M. J. Hu, L. Zhang, S. Aryal, C. Cheung, R. H. Fang, L. F. Zhang, *Proc. Natl. Acad. Sci. USA* **2011**, *108*, 10980; b) L. F. Zhang, J. M. Chan, F. X. Gu, J. W. Rhee, A. Z. Wang, A. F. Radovic-Moreno, F. Alexis, R. Langer, O. C. Farokhzad, *ACS Nano* **2008**, *2*, 1696.
[25] a) S. H. Medina, M. E. H. El-Sayed, *Chem. Rev.* **2009**, *109*, 3141; b) R. K. Tekade, P. V. Kumar, N. K. Jain, *Chem. Rev.* **2009**, *109*, 49; c) S. Zhu, L. Qian, M. Hong, L. Zhang, Y. Pei, Y. Jiang, *Adv. Mater.* **2011**, *23*, H84.
[26] X. P. Ma, J. B. Tang, Y. Q. Shen, M. H. Fan, H. D. Tang, M. Radosz, *J. Am. Chem. Soc.* **2009**, *131*, 14795.
[27] Y. Shen, X. Ma, B. Zhang, Z. Zhou, Q. Sun, E. Jin, M. Sui, J. Tang, J. Wang, M. Fan, *Chem. Eur. J.* **2011**, *17*, 5319.
[28] D. K. Struck, D. Hoekstra, R. E. Pagano, *Biochemistry* **1981**, *20*, 4093.
[29] K. Kono, T. Igawa, T. Takagishi, *Biochim. Biophys. Acta-Biomembr.* **1997**, *1325*, 143.
[30] E. S. Lee, K. Na, Y. H. Bae, *J. Controlled Release* **2005**, *103*, 405.
[31] G. Helmlinger, F. Yuan, M. Dellian, R. K. Jain, *Nat. Med.* **1997**, *3*, 177.